AAS 18-447

RAAN-AGNOSTIC 3-BURN DEPARTURE METHODOLOGY FOR DEEP SPACE MISSIONS FROM LEO DEPOTS

Michel Loucks,[*] Jonathan Goff,[†] John Carrico[‡], Brian Hardy[§]

The authors continue investigation of a 3-burn departure approach that enables deep space missions to depart from a LEO depot even if the depot orbital plane is not optimally aligned with the desired departure asymptote. In this paper, a methodology will be described for targeting specific departure trajectories from a LEO depot whose orbit's RAAN is not optimized for the given mission, and the concept will be illustrated by showing how multiple interplanetary missions can realistically be launched, in a short time-period, from a single LEO depot.

INTRODUCTION: ORBITAL DYNAMICS CHALLENGES OF USING LEO PROPELLANT DEPOTS FOR DEEP SPACE DEPARTURES

Long considered an important enabler in the development of large-scale space architectures, propellant depots have the potential to deliver a variety of strategic and economic benefits to future spacefaring nations. A LEO depot in particular, conveniently located at the first practical stopping point when departing Earth's gravity well, could serve as a key stopping point on the way to higher orbits or beyond-Earth missions. By enabling launch vehicles to refuel on-orbit, or providing propellant for transfer vehicles launched empty, LEO depots are capable of enabling substantial increases in the beyond-Earth payload capacity of contemporary launch vehicles, as well as enabling reusable in-space transportation architectures. Depots also offer a selling point for beyond-Earth ISRU propellant production, as well as provide a base of operations for satellite servicing providers. Together, increased payload capacity and a persistent depot presence are expected to drive markets across the space sector, including:

- Lunar and deep-space departures for government and commercial missions
- Persistent GEO/MEO platforms, delivered via lower-cost distributed launches and then assembled and maintained on-orbit
- In-situ propellant production from the lunar surface or near-Earth asteroids
- Cislunar tourism and orbital settlements

Still, though capable of providing significant increases in payload capacity, propellant depots in LEO face challenges when enabling interplanetary departures. Most notably, as the depot's orbit precesses over time, there is no guarantee that its orbital plane will be properly aligned with a given departure asymptote during an interplanetary transfer window. Previous responses to this problem

[*] President and CEO, Space Exploration Engineering Corp., Friday Harbor, WA loucks@see.com
[†] President and CEO, Altius Space Machines, Broomfield, CO jongoff@altius-space.com
[‡] CTO, Space Exploration Engineering Corp., Ellicott City, MD astrogatorjohn@see.com
[§] 2018 Matthew Isakowitz Fellow, Altius Space Machines, Broomfield, CO brian@altius-space.com

have suggested using multiple depots or phasing the depot orbit between missions, but these solutions are not optimal in many cases and are logistically difficult in others. The use of multiple depots requires increased upfront cost and more complex maintenance logistics, while the latter solution implies that the depot is only able to support one mission at any given time. Rather than force the depot itself to perform phasing maneuvers to accommodate different missions, the authors instead propose a departure methodology utilizing a series of maneuvers to place the departing spacecraft in a phasing orbit properly aligned with the desired departure asymptote so that at the desired departure date, the spacecraft can perform its final departure maneuver as it reaches its phasing orbit periapsis.

In a previous paper [1], the authors demonstrated both a two and three-burn departure method for departure from a LEO depot. The three-burn method, shown in Figure 1 and Figure 2, allows a spacecraft to depart to interplanetary destinations that have a higher declination than the depot, or where the depot isn't properly aligned with the departure asymptote at the desired departure time. This method involves an initial burn (2) to boost the spacecraft into a highly-elliptical phasing orbit, timed to return to perigee at the desired departure date. This perigee also lies on the locus of injection points for the desired interplanetary destination, which can be seen as the white ring in Figure 1. Once at apogee in the phasing orbit, the spacecraft then performs a second maneuver (3) to change planes and align its orbit with the outgoing asymptote. Finally, following the plane-change maneuver and coast back to perigee, the spacecraft performs a third burn (4), to inject itself onto the departure trajectory. Theoretically, the three-burn method can be simplified to a two-burn method when the departure declination is less than the depot inclination. In practice, however, a large phasing orbit is subject solar and lunar perturbations near apogee, which would require a plane adjustment at apogee, thus making any 2-burn departure functionally a 3-burn departure.

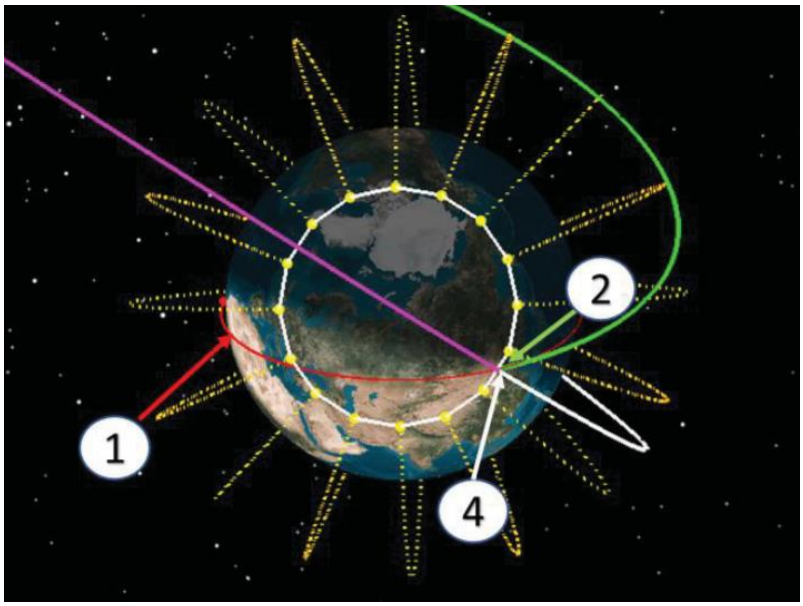

Figure 1: Initial depot orbit & the locus of injection points (reproduced from [1])

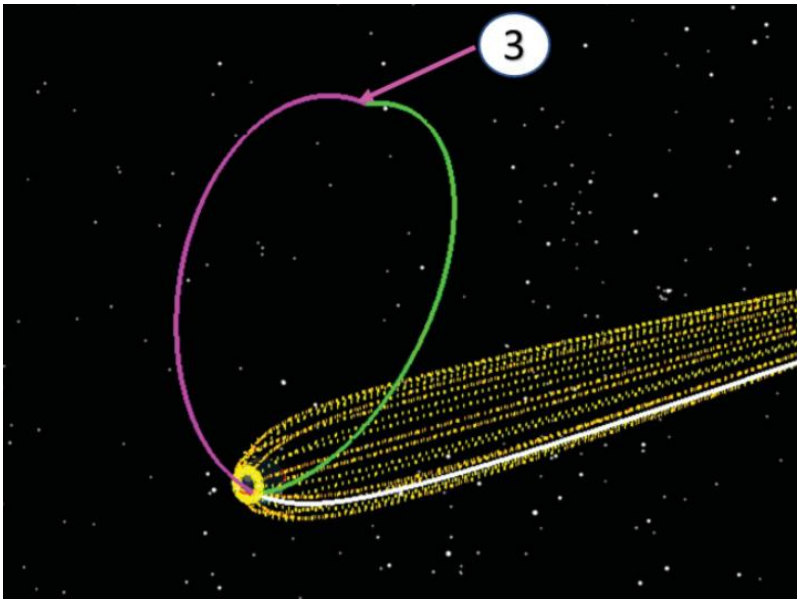

Figure 2: Phasing orbit plane change & insertion onto interplanetary trajectory (reproduced from [1])

The authors' previous work demonstrated the feasibility and ΔV costs of two and three-burn departure methods from a single LEO depot orbit, demonstrating a variety of potential missions that could be achieved from a single depot inclination. Still, the approach was simplistic in that it used a fixed apogee for the phasing orbit, which would still require the depot to phase into the right RAAN prior to the three-burn-departure. We also did not account for the nature of a single physical depot in an existing orbit, and that any departures from such a depot must necessarily leave from the same precessing orbital plane, as dictated by the initial conditions of the depot. In this paper, we have chosen a conceptual depot orbit with an ISS-like set of initial conditions and shown that a series of 8 interplanetary departures is available from this depot over a six-month period. From this case, we extrapolate that many more departures would also be available over longer durations and thus make the case for the general utility of the depot.

RAAN AGNOSTIC 3-BURN DEPARTURE METHODOLOGY

For the simplest optimization strategy, the case of minimum ΔV penalty, an eight-step methodology is outlined below for determining a three-burn departure strategy from a given LEO depot. This methodology inputs a desired interplanetary target, as well as knowledge of the depot RAAN, and then outputs the total required ΔV and the number of Earth passes required for phasing. The steps are outlined here.

1) Identify Ideal Departure Time & Geometry

For a given target, find the optimal interplanetary departure date, hyperbolic asymptote ($\vec{v}_\infty$) vector, along with angular extent of the locus of periapses. The angular extent is defined as

$$Angular\ Extent = \pi - \arccos(^{-1}/_{e})$$

For objects that require a very low energy departure C3, the angular extent of the locus can be very small. In fact, in some cases, the osculating eccentricity of the out-bound trajectory is actually less than 1 (although very nearly 1.0). In these low-energy departure cases the

eccentricity vector can be used as the anti-asymptote vector, which points the apogee, along the line of apsides, at the desired outgoing target. The angular extent of this is then zero. Even when the angular extent is near or at zero, the three-burn algorithm can still be used, if the declination of the departure asymptote is less than the inclination of the depot.

2) Check if a Simple One-Burn Departure is Feasible

If at the time of departure, the $\vec{v}_\infty$ vector is in or very near the depot orbit plane, then a one-burn departure is also possible. This can be determined by verifying that the angle between the depot's angular momentum vector and the $\vec{v}_\infty$ vector is sufficiently small ($\vec{h}_{depot} \cdot \vec{v}_\infty \approx 0$). For a depot not performing phasing maneuvers to align for a particular mission, this occurrence will be rare and does not occur in the examples given in this paper.

3) Calculate the Orbit in Which to Perform the First Maneuver

Propagate the spacecraft in the precessing orbit until the $\vec{v}_\infty$ vector is in the depot's orbit plane, which is when until $\vec{h}_{depot} \cdot \vec{v}_\infty$ reaches a minimum. If the date that the depot orbit precesses to the $\vec{v}_\infty$ vector is less than about 10 days before the departure time, use the previous date that the $\vec{v}_\infty$ was in the depot orbit plane. For the depot in an ISS-like orbit, this is would be about 36 days earlier.

4) Calculate the Time of the First Maneuver

The first maneuver, which will raise apogee, will be performed at the instant that the space-craft crosses from inside the locus of injection points to the outside, during the orbit when the $\vec{v}_\infty$ vector is in or very near the orbit plane.

5) Calculate the Duration to Spend in the Phasing Loops

The duration spent in the phasing loops is the time from the 1st maneuver epoch until the time of departure. The notional depot orbit precesses 180 degrees in 36 days. With a desired minimum phasing loop time of near 10 days, the total duration spent phasing should nor-mally be less than 46 days.

It is possible to create single or multiple phasing loop solutions with an orbit period much longer than 10 days. We've even created some cases with single loop orbit periods of near a month. These orbits, however, are more susceptible to 3rd body perturbations, and it is harder to generalize a solution because of the non-linear effect of intermediate Lunar gravity assists. They are possible in some cases and can be a useful part of the trade-space, when balanced with other logistical constraints. In general, we have attempted to keep the orbit periods near 10 days, and kept the examples from requiring longer than 46 days for phasing.

6) Determine the Number of Phasing Loops

To avoid extra perigee maneuvers we plan for all the phasing loops to have the same orbit period. We calculate the orbit period by dividing the phasing duration evenly so that each loop is around 10 days. This will be from one to four loops.

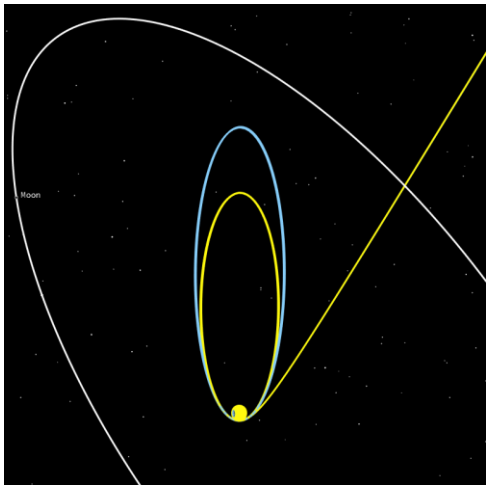

Figure 3. Two-loop (blue) and a Three-Loop (yellow) phasing orbits shown in Inertial Coordinates

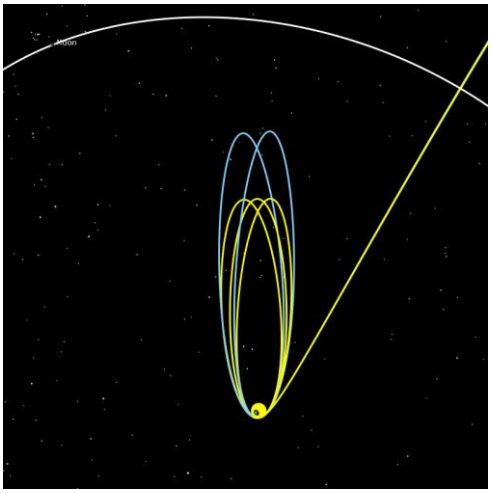

Figure 4. Two-loop (blue) and a Three-Loop (yellow) phasing orbits shown in Earth-Sun Rotating Coordinates

Figure 3 shows an example of a two-loop phasing case (in blue) compared to three-loop phasing case (in yellow.) The same phasing orbits are shown in Figure 4, which is depicted in the Earth-Sun Rotating coordinate system. This rotating system is convenient for such cislunar orbits because the approximately 1-degree per day rotation of the Earth around the Sun separates the orbits so that the number of orbits is more clearly seen than when shown in inertial. These figures demonstrate that because the duration of the entire phasing loop sequence is constant, the strategies with more loops must have shorter orbit periods.

7) Design the Phasing Orbits

We design the phasing loops by calculating the 1st maneuver ΔV such that after all the phasing loops the spacecraft is at perigee at the desired departure time. We use a high-fidelity numerical orbit propagator modeling the 8x8 gravitational field of the Earth, as well as the point-mass gravitational acceleration from the Moon and Sun, whose positions are retrieved dynamically from JPL DE 430 ephemerides. Because the gravity of the Moon and Sun affect such large cislunar orbits, we must adjust the phasing loops with maneuvers in two ways. First, it is important to verify that the perigee is never too low: if any perigee is too low we add a maneuver at the previous apogee to raise perigee to a safe altitude. Second, the Lunar-Solar perturbations sometimes rotate the phasing loop orbit plane, in which case we use a maneuver at apogee to ensure that the outgoing asymptote is correct.

8) Tally the ΔV Values

To calculate the total ΔV for each three-burn departure case, we sum:

a. $\Delta v_{to\ apogee}$: enters the phasing orbit
b. $\Delta v_{plane\ change}$: adjusts the orbit plane at apogee
c. $\Delta v_{correction}$: compensates for Lunar and Solar perturbations during phasing
d. $\Delta v_{departure}$: provides the required escape C_3 at perigee, after any plane change

9) Repeat Steps 6, 7, and 8 for Other Phasing Loop Strategies

Because it is not obvious how the Lunar and Solar perturbations will affect each phasing loop strategy, we create separate cases of 1-4 phasing loops and compare the ΔV values needed to compensate for the perturbations. If there were no perturbations, then the larger phasing loops would lower the departure ΔV (which would be borne by either the spacecraft or the "kick" stage described below) because the orbit energy is already high. However, the larger phasing loops are most susceptible to the third body perturbations from the Moon and Sun, and so by comparing multiple strategies, the minimum ΔV can be found.

Note that the final step of this methodology can be extended further, with more than three phasing loops in the phasing orbit if desired. The addition of more loops with a lowered phasing apogee is ultimately a trade-off, increasing the ΔV penalty for the plane change and the number of Van Allen belt crossings but also decreasing the impact of lunar perturbations. The optimal number of passes is thus strongly influenced by the Moon's location relative to the spacecraft at phasing apogee. Also, it should be mentioned that if too low of a phasing orbit apogee is selected, the RAAN of the phasing orbit could potentially still have some amount of precession, which would need to be factored in during the trajectory planning process.

MISSION EXAMPLE: A FIVE MONTH INTERPLANETARY DEPARTURE BLITZ

Mission Example Overview

As a use case to demonstrate the viability of the RAAN agnostic 3-burn departure methodology, we simulated a campaign of eight interplanetary missions, and one lunar landing mission, departing from a single ISS-coorbital depot over a five-month period, starting in late August 2024, and ending in late January 2025. During a timeframe this short, it would be impractical for the depot to phase its plane to align to the respective departures, and even if it was practical, staying coplanar with the ISS would allow the depot to purchase excess propellants from commercial cargo & crew launches, and enable the possibility of astronauts more conveniently constructing and maintaining the depot. Because the depot cannot phase itself to align optimally for each departure, the RAAN-agnostic 3-burn departure methodology is required to enable these missions.

The desired targets and departure dates for this five-month campaign are shown in Table 1.

Table 1: Targets and Depature Conditions

Trajectory Target	Earth Departure Date	Departure C_3 (km^2/sec^2)
Jupiter	22 Aug 2024	86.9
Mercury	15 Sep 2024	54.9
Moon	26 Sep 2024	-1.99*
Mars	07 Oct 2024	11.12
2008 XB23	02 Nov 2024	0.38
2008 EV5	05 Nov 2024	2.15
Venus	28 Nov 2024	11.32
2001 QJ142	02 Jan 2025	0.65
2009 HC	29 Jan 2025	0.31

* This is the C3 through completion of the TLI burn. After TLI an additional 827 m/s is required to enter a 250km circular altitude polar low lunar orbit, and another 2150m/s required for the lander to go from LLO to the lunar surface. The total mission ΔV from LEO is actually equivalent to a C_3 of approximately 70 km^2/sec^2.

For this simulation, the depot is located in an orbit similar to the International Space Station (ISS): a circular orbit at 400 km altitude, with an inclination of 51.6 degrees, and to simplify things, we chose an arbitrary RAAN for the ISS and the depot of zero degrees on August 1st, 2024. We used an 8x8 gravity field in the low-Earth orbit which causes the RAAN to precess westward by about 5 degrees per day.

We used standard pork-chop plots to identify representative (although not necessarily optimal) transfers to each of these planets and asteroids. By selecting departure dates so close together it would not be feasible to phase the depot's orbit to align for a 1-burn departure in every case. If the depot were, indeed, co-orbiting with the ISS, it would be much less likely that the depot and ISS would be able to phase for specific departure dates.

Figure 5: Centaur V-Derived SmallSat Propellant MicroDepot (Credit: Brian Versteeg)

Figure 5 shows a concept for the LEO depot that is used in this campaign scenario. This LEO MicroDepot is sized to refuel the upper stage of dedicated smallsat launch vehicles, such as Virgin Orbit's LauncherOne rocket, as well as storable kick stages, spacecraft, and lander stages. This microdepot concept is a based on reusing the LOX tank from a Centaur V upper stage after it has placed a primary payload (such as Cygnus cargo vehicle) into orbit, combined with a depot kit mounted as a secondary payload between the Centaur V stage and the primary payload. The kerosene tank for refueling the small rocket upper stages, and the storable propellant tanks for fueling the kick stages and/or lander stages are part of the depot kit section. The depot kit also includes multiple capture and refueling arms allowing both capture of delivery stages for refueling the depot itself, as well as for capturing small rocket upper stages with attached payloads and kick stages that will be receiving propellant from the depot.

Upper Stage/Kick Stage/Lander Capabilities

To better quantify the mission payload performance enabled by a three-burn departure from a LEO depot, additional work was undertaken to approximate the specifications of representative launch vehicles, kick stages, and lunar landers. This allows us to quantify the payload mass that could be delivered to the various interplanetary targets, and the lunar surface.

Specifically, the study focused on the use of Virgin Orbit's LauncherOne vehicle both for initial delivery of the payload stack to LEO and then after refueling at the depot, for insertion into the departure phasing orbit. We also modeled a generic storable bi-propellant kick stage to enable plane changes and other perturbation corrections at the apogees of the phasing orbits, and for the final Earth departure maneuver. Lastly, for lunar missions we assumed the kick stage would also perform the Lunar Orbit Insertion burn, and we modeled a notional storable lander stage used for placing payloads onto the lunar surface. LauncherOne was selected as a representative smallsat launcher upper stage because it is roughly in the middle of the payload range for proposed small launch vehicles, though this same technique should also work for the upper stages of other smallsat launch vehicles like the RocketLab Electron or the Firefly Alpha vehicles.

The LauncherOne vehicle, slated for its first test flight later this year, is assumed to transport the empty kick stage, empty lander stage (for lunar landing missions), and a payload first to LEO. Once in LEO the integrated stack including LauncherOne upper stage plus storable stage(s) and payload would rendezvous with the depot, and then after the LauncherOne upper stage and storable stage(s) are refueled, the stack would then perform the 3-burn departure maneuver.

To estimate the capabilities of the LauncherOne upper stage, shown below in Table 2, a variety of public sources were used to either locate or interpolate data. The maximum propellant load is based on information provided in the FAA's Final Environment Assessment for Launcher One [1], and the vehicle's maximum payload capability to a low-inclination, 400-km orbit was found in the latest LauncherOne Service Guide [3]. An estimated structural coefficient and specific impulse were then interpolated from data on comparable vehicles, including Falcon 1e and Electron, which allows us to approximate the upper stage's structural mass.

Table 2: Estimated Upper Stage/Kick Stage Capabilities [1] [3]

	Structural Coefficient	**Structural Mass**	**Specific Impulse**	**Max. Propellant Load**	**Max. Payload to ISS Orbit**
LauncherOne Upper Stage	0.12	329.3 kg	325 s	2415 kg	475 kg
Storable Kick Stage	0.25	Variable	310 s	Variable	N/A
Storable Lander Stage	0.40	Variable	310 s	Variable	N/A

Following the upper stage burn to enter the phasing orbit, the LauncherOne stage will separate from the conjoined storable stage(s) and payload. This custom kick stage, launched either dry or fueled, is assumed to perform the two remaining burns to change orbit planes and depart Earth. If launched dry, the kick stage will refuel at the LEO depot in tandem with the LauncherOne upper stage. Estimated capabilities of the custom kick stage, including the structural coefficient and specific impulse shown in Table 2, are based on recent conversations with colleagues in the propulsion industry, including those at Tesseract and Deep Space Industries. A kick stage is necessary because the LauncherOne upper stage, like most other similar cryogenic upper stages, is unable to operate for more than a few hours after leaving the depot. For lunar lander missions, the storable kick stage would also perform the Lunar Orbit Insertion burn, and the storable lander stage would perform the descent from LLO and the final landing maneuver. The performance of the storable lander stage was based on using a similar storable propulsion system to the kick stage, but with the addition of landing gear and landing sensors negatively impacting the structural coefficient. It should be noted that unlike the LauncherOne upper stage, both the structural mass and maximum propellant load

for the two storable stage types are assumed to be completely scalable. In reality as the stage size increases, the structural fraction should significantly improve, but for the case of this study, we used a constant structural fraction to simplify things.

Given a series of 3-burn results, the estimated stage capabilities in Table 2 allow one to size all of the stages appropriately to determine the maximum potential payload mass to a destination. Throughout this staging analysis, detailed below, it is assumed that the LauncherOne upper stage has a fixed structural mass but that its propellant load may vary when refueled in LEO. The storable kick and lander stages are assumed to be scalable to whatever structural mass and propellant load is required, so long as the structural coefficient is maintained. Sizing is based only on required burns after arrival at the LEO depot, and on the LauncherOne's overall LEO payload capability.

Knowing the total ΔV that each stage must provide post-refueling and the estimated I_{sp} of each, one first determines MF_{US} and MF_{KS}, the required mass fractions for the upper stage and kick stage, respectively. Next, the initial mass of the kick stage with payload, $m_{0,\ KS}$, is set based on the kick stage's launch configuration. A kick stage that is fully fueled at launch will require LauncherOne to carry the kick stage propellant and structure as well as the payload into LEO. When the kick stage is launched dry, however, only its structural mass and the payload must be moved to LEO.

$$m_{0,\ KS} = \begin{cases} max(m_{L,\ US,\ to\ LEO}) & if\ kick\ stage\ launched\ wet \\ MF_{KS}\ \cdot\ max(m_{L,\ US,\ to\ LEO}) & if\ kick\ stage\ launched\ dry \end{cases}$$

Note that in all cases m_0 refers to the mass of an entire stage plus all stages/payloads above it, at the time of its first burn after depot rendezvous/refueling. Once the initial mass of the kick stage with payload is known, its fixed mass fraction MF_{KS} and structural coefficient ε_{KS} are used to back out the stage's propellant mass $m_{p,\ KS}$, structural mass $m_{s,\ KS}$, and payload mass $m_{L,\ KS}$.

$$m_{p,\ KS} = \left(1 - \frac{1}{MF_{KS}}\right) m_{0,\ KS}$$
$$m_{s,\ KS} = \left(\frac{\varepsilon_{KS}}{1 - \varepsilon_{KS}}\right) m_{p,\ KS}$$
$$m_{L,\ KS} = m_{0,\ KS} - m_{p,\ KS} - m_{s,\ KS}$$

Next, recognizing that the initial mass of the kick stage with payload is also the payload mass for the LauncherOne upper stage, the upper stage's payload mass $m_{L,\ US}$ and propellant mass $m_{p,\ US}$ can both be determined. Recall that the upper stage structural mass $m_{s,\ US}$ is assumed to be fixed at the value shown in Table 2.

$$m_{L,\ US} = m_{0,\ KS}$$
$$m_{p,\ US} = (MF_{US} - 1)(m_{s,\ US} + m_{L,\ US})$$

Finally, the newly-calculated upper stage propellant mass is compared to the actual capabilities of LauncherOne. If this mass $m_{p,\ US}$ is less than the maximum propellant load of the LauncherOne upper stage, the upper stage will not need to be fully refueled in LEO, and one may omit the remaining calculations in this section. If $m_{p,\ US}$ exceeds the maximum propellant load, however, both stages must be resized accordingly.

$$m_{p,\ US} = \max(m_{p,\ US})$$
$$m_{L,\ US} = \frac{m_{p,\ US}}{MF_{US} - 1} - m_{s,\ US} \qquad if\ m_{p,\ US} > \max(m_{p,\ US})$$
$$m_{0,\ KS} = m_{L,\ US}$$

Once the initial mass of the kick stage with payload was been redefined, one can repeat previous steps to recalculate the new propellant, structural, and payload masses for the kick stage. Both

stages are thus sized such that the maximum propellant load of the LauncherOne upper stage is not exceeded. In the case of a lunar landing mission, a similar set of calculations can be performed, but with the additional lander stage included.

With the above calculations complete, the propellant, structural, and payload masses for all three stages are completely defined. The payload mass of the kick stage, $m_{L,\ KS}$, represents the usable payload that can be delivered onto the desired interplanetary trajectory.

Departure Blitz Results

The following tables contain the results of the targeted trajectories in the departure blitz. The first column of each table row is the number of phasing loops used. The second column is the ΔV value calculated for the first maneuver, which raises the apogee. The third column is the ΔV sum of any and all maneuvers performed at the phasing loop apogee(s) to control the perigee radius and the orbit plane rotation. The fourth column contains the ΔV needed to transfer from the phasing loop to the departure trajectory. For the interplanetary missions, the fifth column is the propellant mass of the refueled upper stage based on the method and assumptions described in the previous subsection. Likewise, the sixth column contains the propellant mass for the kick stage, and the seventh column is the final payload mass delivered on the outbound trajectory. The last column is the orbital period in days of the phasing orbit. In the case of the lunar mission, additional columns were added for the LOI and Landing ΔV, and the lander propellant load.

Table 3: 3-Burn Maneuver Characteristics (Jupiter, Aug. 2024 Opportunity)

# Loops	ΔV, Raise Apogee (m/s)	ΔV, Plane Change & Correct. (m/s)	ΔV, Injection (m/s)	Prop. Mass, Upper Stage (kg)	Prop. Mass, Kick Stage (kg)	Payload Capacity (kg)	Orbit Period (days)
1	3128.573	53.445	3487.302	2415	769	92	25.892
2	3098.175	69.166	3514.773	2415	789	88	12.955
3	3073.914	61.616	3539.384	2415	804	86	8.647

Table 4: 3-Burn Maneuver Characteristics (Mercury, Sept. 2024 Opportunity)

# Loops	ΔV, Raise Apogee (m/s)	ΔV, Plane Change & Correct. (m/s)	ΔV, Injec-tion (m/s)	Prop. Mass, Upper Stage (kg)	Prop. Mass, Kick Stage (kg)	Payload Capac-ity (kg)	Orbit Period (days)
1	3132.512	81.642	2319.047	2300	571	285	29.242
2	3106.017	63.181	2345.713	2274	574	284	14.682
3	3082.789	47.755	2368.625	2252	577	283	9.801

Table 5: 3-Burn Maneuver Characteristics (Lunar Landing, Sep. 2024 Opportunity)

# Loops	ΔV, Raise Apogee (m/s)	ΔV, Plane Change & Correct. (m/s)	ΔV, TLI (m/s)	ΔV, LOI (m/s)	ΔV, Landing (m/s)	Prop Mass, US (kg)	Prop Mass, KS (kg)	Prop Mass, Lander (kg)	Net Payload (kg)
2	3087.56	0	4.58	827.42	2150	2415	274.9	396.3	119.2

Table 6: 3-Burn Maneuver Characteristics (Mars, Oct. 2024 Opportunity)

# Loops	ΔV, Raise Apogee (m/s)	ΔV, Plane Change & Correct. (m/s)	ΔV, Injection (m/s)	Prop. Mass, Upper Stage (kg)	Prop. Mass, Kick Stage (kg)	Payload Capacity (kg)	Orbit Period (days)
1	3095.389	42.829	579.236	1497	108	439	12.226
2	3047.432	35.870	628.470	1474	116	436	6.112
3	3006.999	12.906	668.977	1449	119	435	4.074

Table 7: 3-Burn Maneuver Characteristics (2008 XB23, Nov. 2024 Opportunity)

# Loops	ΔV, Raise Apogee (m/s)	ΔV, Plane Change & Correct. (m/s)	ΔV, Injection (m/s)	Prop. Mass, Upper Stage (kg)	Prop. Mass, Kick Stage (kg)	Payload Capacity (kg)	Orbit Period (days)
1	3117.185	66.619	76.967	1373	23	467	21.317
2	3081.342	48.138	112.359	1353	26	466	9.915
3	3051.862	29.140	140.796	1335	27	466	6.609

Table 8: 3-Burn Maneuver Characteristics (2008 EV5, Nov. 2024 Opportunity)

# Loops	ΔV, Raise Apogee (m/s)	ΔV, Plane Change & Correct. (m/s)	ΔV, Injection (m/s)	Prop. Mass, Upper Stage (kg)	Prop. Mass, Kick Stage (kg)	Payload Capacity (kg)	Orbit Period (days)
1	3124.453	22.346	150.097	1386	28	466	24.755
2	3093.544	58.611	176.690	1381	38	462	12.376
3	3069.722	128.989	204.601	1392	55	457	8.251

Table 9: 3-Burn Maneuver Characteristics (Venus, Nov. 2024 Opportunity)

# Loops	ΔV, Raise Apogee (m/s)	ΔV, Plane Change & Correct. (m/s)	ΔV, Injection (m/s)	Prop. Mass, Upper Stage (kg)	Prop. Mass, Kick Stage (kg)	Payload Capacity (kg)	Orbit Period (days)
1	3100.765	47.449	631.928	1519	119	435	16.138
2	3062.176	68.022	611.987	1490	119	435	8.057

3	3030.007	39.839	645.755	1468	120	435	5.371

Table 10: 3-Burn Maneuver Characteristics (2001 QJ142, Jan. 2025 Opportunity)

# Loops	ΔV, Raise Apogee (m/s)	ΔV, Plane Change & Correct. (m/s)	ΔV, Injection (m/s)	Prop. Mass, Upper Stage (kg)	Prop. Mass, Kick Stage (kg)	Payload Capacity (kg)	Orbit Period (days)
1	3119.234	16.692	86.555	1363	16	470	19.017
2	3081.447	47.584	124.905	1356	28	466	9.512
3	3049.765	43.978	154.632	1341	32	464	6.337

Table 11: 3-Burn Maneuver Characteristics (2009 HC, Jan. 2025 Opportunity)

# Loops	ΔV, Raise Apogee (m/s)	ΔV, Plane Change & Correct. (m/s)	ΔV, Injection (m/s)	Prop. Mass, Upper Stage (kg)	Prop. Mass, Kick Stage (kg)	Payload Capacity (kg)	Orbit Period (days)
1	3118.578	49.449	94.670	1374	23	467	22.832
2	3088.087	35.120	97.365	1350	21	468	11.388
3	3061.213	24.771	123.906	1336	24	467	7.597

CONCLUSION

The results demonstrate that the 3-burn departure strategy can enable nine spacecraft to depart for nine different interplanetary targets using a single propellant depot in an ISS-like orbit, where the depot does not perform any phasing maneuvers to align with any of the departure asymptotes. The cislunar phasing orbits were able to successfully compensate for the fact the depot orbit does not cross the departure asymptote at the desired departure time. Even though the phasing orbits have high apogees, susceptible to Lunar and Solar gravity perturbation, only small maneuvers were needed to control the orbit.

The advantages of LEO refueling are also evident in the results, allowing a LauncherOne-class vehicle, which normally would not be useful for interplanetary missions to send payloads larger than 400kg to most interplanetary destinations, and even send useful microsatellite-class payloads to Mercury, Jupiter, and the Lunar surface. This enables extending the economic benefits of dedicated smallsat launch to interplanetary missions.

Ephemerides are available from the authors upon request in a variety of formats. Additional information may be found on the Astrogator's Guild blog at: www.astrogatorsguild.com which is managed by authors Carrico and Loucks.

FUTURE WORK

During the course of this research, we identified several avenues for follow-on work:

- There are some cases we discovered with very low departure energies, including some with a C_3 slightly less than zero. We plan to look more into these cases and have already started looking at transfers to the Moon, which also fall into this class.

- Future work can also be used on lunar missions to more fully show when such phasing orbit techniques are useful, such as missions that involve rendezvousing with a depot or facility in a low lunar orbit.

- While tables 3 through 11 show mostly minor apogee maneuver delta-v costs for an arbitrary initial RAAN, it would be useful to identify the worst-case scenario by scanning through 180 degrees of RAAN for any of these cases, in order to help quantify the magnitude of the ΔV and flight-time penalties of using this 3-burn departure approach.

- In addition, there are cases with very high (or very low) declinations such that the latitude of the asymptote minus the angular extent is greater than the inclination of the LEO, in which case the 3-burn algorithm doesn't work. We believe a similar multi-burn transfer will work by rotating the line of apsides with maneuvers and/or using the Lunar and Solar perturbations to align the perigee for the hyperbolic departure.

- Lastly for mission optimization utilizing 3-burn departure maneuvers, it may be helpful to also look at gravity assist maneuvers, missions that transition to low-thrust/high-Isp propulsion after escape, or missions that use multiple kick stages for high-C_3 missions.

- It may also be interesting to investigate the opposite of the 3-burn departure method for enabling a 3-burn arrival, when it's necessary to rendezvous with a depot or other facility at the far end of an interplanetary mission.

ACKNOWLEDGEMENTS

We would like to thank Josh Hopkins of Lockheed Martin Corporation and Chris Lewicki of Planetary Resources, Inc., for suggesting interesting interplanetary targets and their timing, and Grant Bonin of Deep Space Industries, and Erik Franks and Jacob Teufert of Tesseract for sharing projected capabilities of their respective storable kick stage systems for use in the analysis.

REFERENCES

[1] Federal Aviation Administration, "Final Environmental Assessment and Finding of No Significant Impact for Issuing a License to Virgin Orbit (LauncherOne), LLC for LauncherOne Launches at the Mojave Air and Space Port, Kern County, California," 2017.

[2] M. Loucks, J. Goff and J. Carrico, "Practical Methodologies for Low Delta-V Penalty, On-Time Departures to Arbitrary Interplanetary Destinations from a Medium-Inclination Low-Earth Orbit Depot," AAS, 2017.

[3] Virgin Orbit, "LauncherOne Service Guide," August 2018. [Online]. Available: https://static1.squarespace.com/static/5915eeab9de4bb10e36a9eac/t/5b68cc438a922d4579cb760b/1533594696524/ServiceGuide_1.1_web_080618.pdf. [Accessed 10 August 2018].